Electronic Supplementary Material (ESI) for Physical Chemistry Chemical Physics.
This journal is © the Owner Societies 2022

Supporting Information

Prediction of highly stable two-dimensional materials of boron and phosphorus: structural and electronic properties

Puxin Cheng,[a] Geng Li,[*a,b] Shuming Zeng,[c] Yunlong Li,[b] Xiangfei Meng,[b] and Jialiang Xu[*a]

[a] *School of Materials Science and Engineering, National Institute for Advanced Materials, Nankai University, Tongyan Road 38, Tianjin 300350 (P. R. China),*

E-mail: jialiang.xu@nankai.edu.cn.

[b] *National Supercomputer Center in Tianjin, Tianjin 300457 (China),*

E-mail: ligeng@nscc-tj.cn.

[c] *Department of Physics, Yangzhou University, Yangzhou 225009, China.*

Table of Contents

1. Calculation Methodology

The elastic moduli C_{ij} of $P2_1/m$ B_1P_3 and Cm B_2P_4 have been obtained from strain-energy relationship to investigate the mechanical property.[1] In the calculations, we have set seven different levels of applied strain to improve the accuracy, including positive strain (stretching the primitive cell), +1%, +2%, +3%, and negative strain (compressing the primitive cell), −1%, −2%, −3%. Other structural properties, such as, Bulk modulus *K*, Young's modulus *E*, Shear modulus *G* and Poisson ratio *υ* (Table S1), can be obtained by the following formulas on the basis of Voigt-Reuss-Hill (VRH) approximation:[1, 2]

$$K = \frac{K_V + K_R}{2}$$

$$E = \frac{9KG}{3K + G}$$

$$G = \frac{G_v + G_R}{2}$$

$$\upsilon = \frac{3K - 2G}{2(3K + G)}$$

Among them, $K_V = \frac{1}{9}(C_{11} + C_{22} + C_{33}) + \frac{2}{9}(C_{12} + C_{13} + C_{23})$, $K_R = \frac{1}{(S_{11}+S_{22}+S_{33})+2(S_{12}+S_{13}+S_{23})}$ and

$G_V = \frac{1}{15}(C_{11} + C_{22} + C_{33} - C_{12} - C_{13} - C_{23}) + \frac{1}{5}(C_{44} + C_{55} + C_{66})$,

$G_R = \frac{15}{4(S_{11}+S_{22}+S_{33})-4(S_{12}+S_{13}+S_{23})+3(S_{44}+S_{55}+S_{66})}$,

where C_{ij} and S_{ij} are elastic constants and elastic compliances, respectively.

The intrinsic carrier mobility (μ) and relaxation time (τ) of $P2_1/m$ B_1P_3 and Cm B_2P_4 have been calculated to investigate the electronic and charge-transport properties. The calculations are based on deformation potential (DP) theory and the used formula is as follows:[3]

$$\mu = \frac{e\tau}{m^*} = \frac{e\hbar^3 C}{k_B \mathrm{T} m^* m_d (E_1)^2}$$

Thus, we have studied the fundamental DP parameters (elastic constant *C*, deformation potential constant E_1, charge effective mass m* and the average effective mass m_d). Among them, *C* is defined as $C = \frac{\partial^2 E}{S_0 \partial(\Delta l/l)^2}$, in which *E* denotes as the total energy of the compounds under ***a***- and ***b***-axis uniaxial strain. E_1 is get from the equation as $E_1 = \frac{\partial E_{edg}}{\partial(\Delta l/l)}$, where E_{edg} is the energy shift of CBM and VBM considering the vacuum level correction.[4] m^* and m_d are defined as $m^* = \frac{\hbar^2}{\partial^2 E/\partial K^2}$ and $m_d = \sqrt{m_x^* m_y^*}$, respectively.[5]

2. Mechanical Properties

$P2_1/m$ B_1P_3 is a monoclinic structure and has four independent elastic constants C_{11}, C_{12}, C_{22} and C_{66}. The mechanical stability criteria are $C_{11} > 0$, $C_{66} > 0$ and $C_{11} \times C_{22} > C_{12} \times C_{12}$.[6] Though Cm B_2P_4 also belongs to a monoclinic space group, their corresponding point groups are different and additional criteria is needed for Cm B_2P_4, namely det (C_{ij}) > 0. It has been confirmed that two compounds are both mechanically stable for satisfying the Born-Huang criteria.[7] *E*, *K* and *G* characterize the hardness of materials, the ability to resist volume and shape change, respectively. As shown in Table S1, both of the values of *E* are higher than MoS_2 (122–126 N/m),[8] but lower than that of graphene (330–348.1 N/m).[9] In addition, the values of *υ* are similar to that of graphene (0.15–0.19) lower than the critical

value 1/3,[10-12] which indicate the brittle nature of the compounds.[13] Furthermore, 2D polar diagram for *E*, *G* and *υ* are displayed in Fig. 6 for the purpose of visualizing the anisotropy of two compounds. The closer the shape is to a circle, the stronger the isotropy. It can be found that $P2_1/m$ B_1P_3 is almost isotropic, while *Cm* B_2P_4 possesses weak anisotropy.

Table S1. Calculated elastic constants C_{ij} (N m^{-1}), Bulk modulus *K* (N m^{-1}), Young's modulus *E* (N m^{-1}), Shear modulus *G* (N m^{-1}) and Poisson ratio *υ* of $P2_1/m$ B_1P_3 and *Cm* B_2P_4.

	C_{11}	C_{12}	C_{16}	C_{22}	C_{26}	C_{66}	*K*	*E*	*G*	*υ*
$P2_1/m$ B_1P_3	193.171	25.688	—	188.977	—	82.656	108.374	187.620	82.672	0.135
Cm B_2P_4	179.726	37.545	-0.611	215.289	−13.839	77.478	116.759	196.335	78.206	0.189

3. Charge-transport Properties

To study the charge-transport performance of $P2_1/m$ B_1P_3 and *Cm* B_2P_4, DP parameters have been calculated and listed in Table S2. As shown in Fig. 5(a), the CBM and VBM of $P2_1/m$ B_1P_3, are located at S and Γ points, respectively, and the flat bands around Γ may contribute to the larger hole effective mass (m_h) than electron effective mass (m_e) in both ***a***- and ***b***-directions, leading to neglective carrier mobility. Furthermore, *m** is anisotropic along different directions in reciprocal space. For *Cm* B_2P_4, the CBM and VBM are located at N and M, respectively. Distinctly, m_e is smaller than m_h in the ***a***-axis but it is adverse in the ***b***-axis. There are two other essential related factors, E_1 and *C*, and both of them are anisotropic, as shown in Fig. S1, in which (a) and (b) display total energy of the compounds as a function of uniaxial direction. For $P2_1/m$ B_1P_3, the value of *C* in the ***a***-axis is slightly larger than that in the ***b***-axis, while that of *Cm* B_2P_4 is opposite. The energy shifts of CBM and VBM under uniaxial strain along the ***a***-and ***b***-axis are shown in Fig. S1 (c) and (d). Consequently, the predicted values of μ are obtained. Excitedly, the electron mobility of $P2_1/m$ B_1P_3 in the ***b***-axis is 13 times higher than that of MoS_2 (10–400 cm^2 V^{-1} s^{-1}) and 5 times higher than that of BP (200–1000 cm^2 V^{-1} s^{-1}).[14-18] *Cm* B_2P_4 exhibits superior electron mobility than that of $P2_1/m$ B_1P_3 especial in the ***a***-axis, which is 32 times higher than that of MoS_2 and 13 times higher than that of BP.

Table S2. The deformation potential constant E_1, elastic constant *C*, hole (electron) effective mass *m** (m_e), hole (electron) mobilities and relaxation time for $P2_1/m$ B_1P_3 and *Cm* B_2P_4 at 300 K.

	Carrier Type	E_1 (eV)	*C* (J m^{-2})	*m** (m_e / m_h)	μ (cm^2 V^{-1} s^{-1})	τ (fs)
$P2_1/m$ B_1P_3	e-***a***	−5.597	98.556	m_{SX} = 0.351 m_0	692.610	151.941
		−5.597	98.556	m_{SY} = 0.217 m_0	1120.304	151.941
	e-***b***	1.940	93.684	m_{SX} = 0.351 m_0	5479.968	1202.168
		1.940	93.684	m_{SY} = 0.217 m_0	8863.911	1202.618
	h-***a***	−3.287	98.556	$m_{ΓS}$ = 1.501 m_0	10.173	9.544
		−3.287	98.556	$m_{ΓY}$ = 108.123 m_0	0.141	9.544
	h-***b***	−1.234	93.684	$m_{ΓS}$ = 1.501 m_0	68.614	64.368
		−1.234	93.684	$m_{ΓY}$ = 108.123 m_0	0.953	64.368
Cm B_2P_4	e-***a***	−1.125	88.962	m_{NH} = 0.343 m_0	13129.968	2814.737
		−1.125	88.962	m_{NY} = 0.323 m_0	13942.969	2814.737
	e-***b***	−1.745	111.389	m_{NH} = 0.343 m_0	6833.066	1464.838
		−1.745	111.389	m_{NY} = 0.323 m_0	7256.166	1464.838
	h-***a***	−3.760	88.962	$m_{MΓ}$ = 0.253 m_0	2228.079	352.315
		−3.760	88.962	m_{MX} = 0.224 m_0	2516.536	352.315
	h-***b***	1.851	111.389	$m_{MΓ}$ = 0.253 m_0	11511.483	1820.253
		1.851	111.389	m_{MX} = 0.224 m_0	13001.809	1820.253

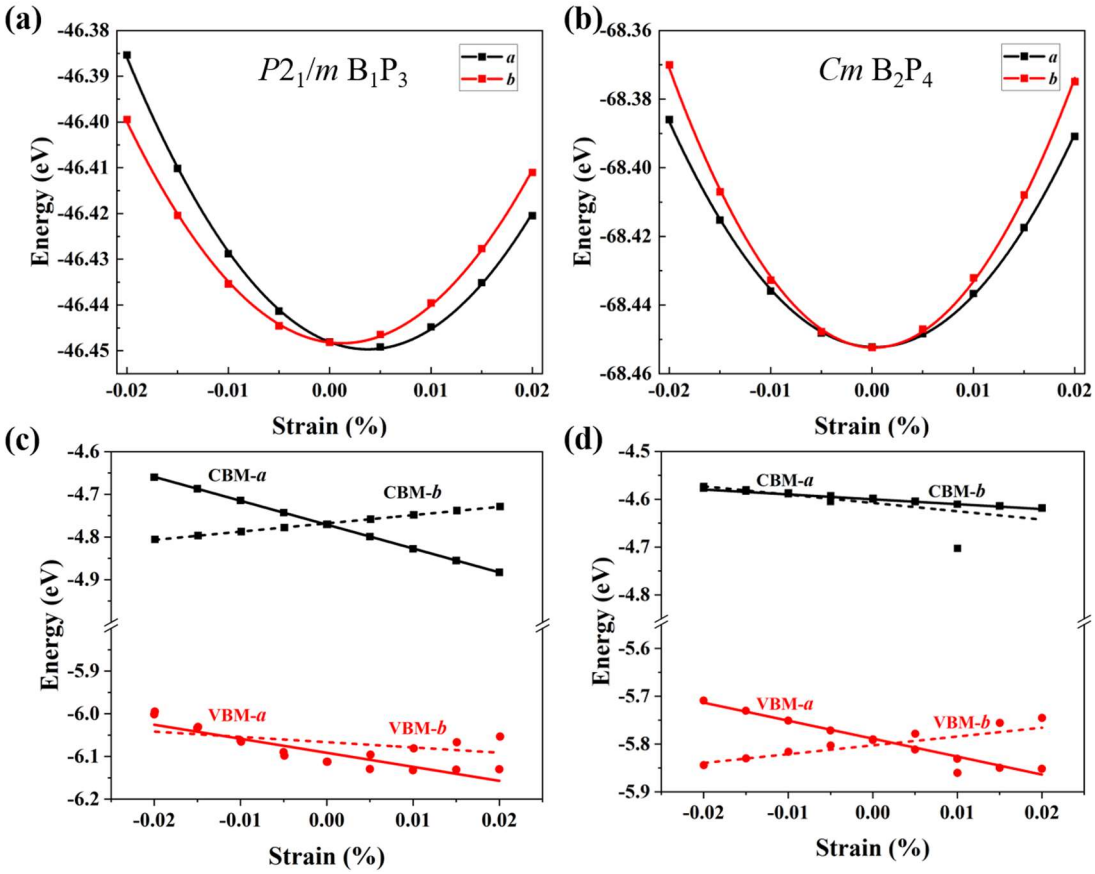

Fig. S1. DP parameters using GGA-PBE functional. (a, b) Total energy of a primitive cell as a function of lattice deformation along the ***a***-and ***b***-axis. (c, d) The energy shifts of CBM and VBM under uniaxial strain along the ***a***- and ***b***-axis.

4. Electronic Properties and Magnetism Under External Modifications

As presented in Fig. 5(a), $P2_1/m$ B_1P_3 has high DOS around E_F, which means its exchange splitting energy is larger than the loss in kinetic energy. Based on Stoner criterion, this compound could appear spontaneous ferromagnetism by doping holes.[19] Consistent with prediction, $P2_1/m$ B_1P_3 transforms into a ferromagnetic ground state at critical hole densities, as shown in Fig. S4(b). The magnetic moments of other compounds under charge doping are also studied and shown in Fig. S4(b). Meanwhile, it should be noted that B_mP_n keep their semiconducting properties in the range studied, except for *Pmma* B_1P_1, which keeps metallic properties in the study range. *Cm* B_2P_4 and $Pmn2_1$ BS-B_1P_1 have similar electronic energy bands, which may contribute to the similar change of magnetic moments upon charge doping. Both of them behave as ideal half-metallic phases with 100% spin polarization around E_F at specific charge doping level. Particularly for $Pmn2_1$ BS-B_1P_1, a small step of magnetic moments appears when the electron doping level < 0.2 per cell, which means it can maintain the fully spin polarization state within a range. For $P3m1$ BH-B_1P_1, the ratio of spin polarization can also reach 100% during doping 0.05 – 0.1 electron into one unit cell. For P-$6m2$ PH-B_1P_1, the magnetic moments fluctuate in a small range (< 0.2 μ_B/charge) under charge doping. These structures have been confirmed with the potential applications in magnetic semiconductors.

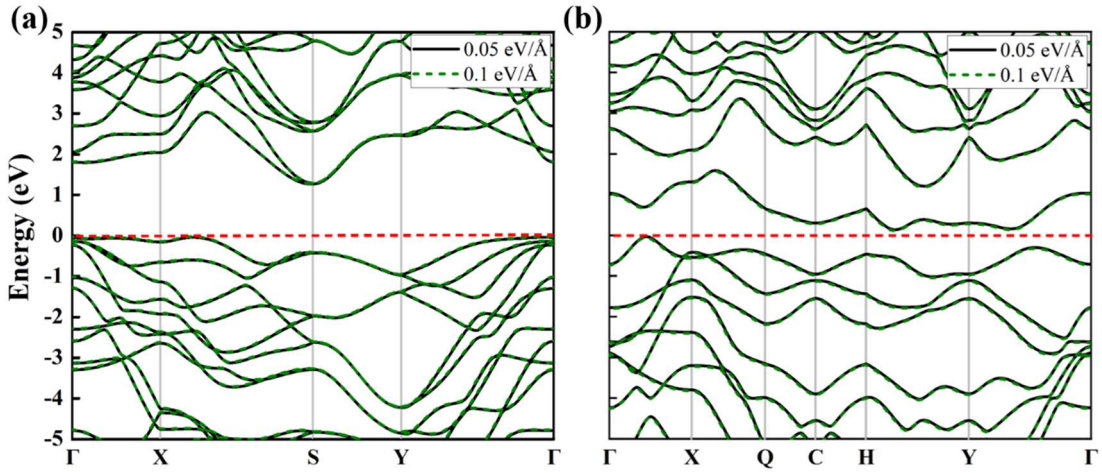

Fig. S2. The band structure of $P2_1/m$ B_1P_3 and Cm B_2P_4 under an external electric field along normal direction.

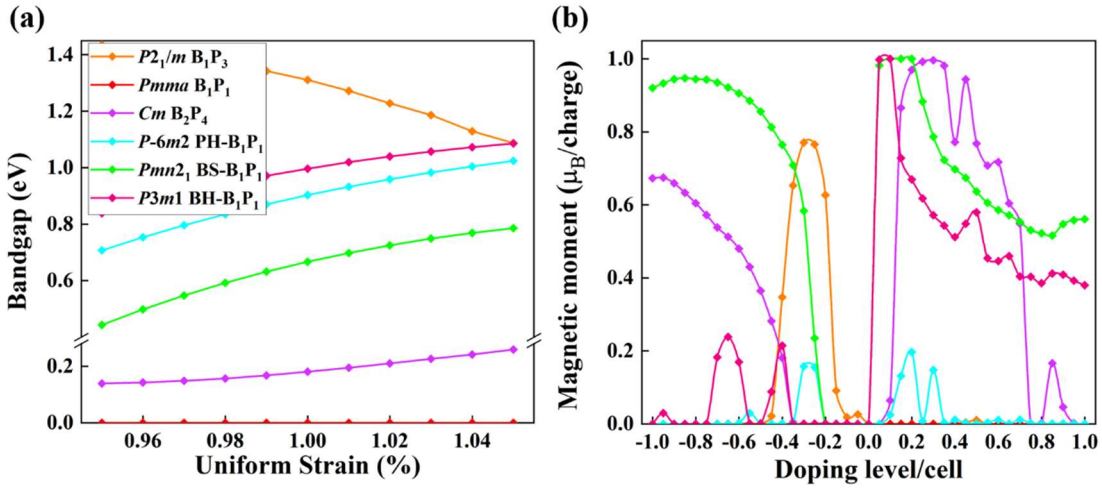

Fig. S3. (Color online) (a) The bandgaps as a function of uniform strain at GGA-PBE level. (b) The magnetic moments of charge-doped B_mP_n. The points represent the actual calculated values, and straight lines are the fit trends.

5. Cartesian Coordinates

Table S3. The Cartesian coordinates of optimized structures of Fig. 2.

$P2_1/m$ B_1P_3	P	5.433231252	0.787032559	8.877891939
	P	0.831709114	2.416798578	7.808816239
	P	1.666625133	0.786952138	5.073872223
	P	3.643400212	0.786911038	6.037181691
	P	2.808472324	2.416715073	8.772065752
	B	4.687858211	2.416699918	4.968145763
	B	0.820792672	2.416657112	5.872357590
	B	3.654305038	0.786970871	7.973599974
$Pmma$ B_1P_1	P	1.194920897	1.595119715	7.172534973
	P	0.000000000	1.595119715	3.550620434
	B	1.194920897	0.000000000	6.045477576
	B	0.000000000	0.000000000	4.677665503
Cm B_2P_4	P	1.067229112	2.000346826	5.727902156

	P	1.858836774	0.594916960	3.890544678
	P	4.126753998	1.398471662	4.846620499
	P	2.314434298	2.500764063	3.181123816
	B	2.354160938	0.750679268	5.148728656
	B	-1.056074346	2.988373182	4.078145986
P-6*m*2 PH- B_1P_1	P	0.000000000	0.000000000	9.970239639
	B	0.000000000	1.854874675	9.970239639
Pmn2_1 BS-B_1P_1	P	1.599130034	0.666851680	6.578180194
	P	0.000000000	3.318391642	7.500000000
	B	0.000000000	0.000000000	7.500000000
	B	1.599130034	2.651540041	6.578180194
*P*3*m*1 BH-B_1P_1	P	0.000000000	0.000000000	7.500000000
	B	-0.000001054	1.856758401	8.156234622

6. Comparison with B_mN_n

Since N atom and P atom are isolobal, we have compared the structures of B_mN_n with the corresponding structures of B_mP_n. Wang *et al.* have reported some energetically stable single layer B_mN_n compounds with various chemical composition (B_2N_3, B_3N_4 and B_3N_5) based on the particle swarm optimization (PSO) algorithm.[20] The bandgaps of all B_mN_n are larger than those of our identified B_mP_n. It is different between the structures of B_2N_3, B_3N_4 and B_3N_5 and *P*-6*m*2 PH-B_1P_1, *Pmn*2_1 BS-B_1P_1 and *P*3*m*1 BH-B_1P_1, though they are all planer structures. The former consists of five-, six-, seven- and eight-membered rings of B-N, but the latter is constructed by only six-membered rings of B-P. Both Li *et al.* and Liu *et al.* have reported pentagonal B_mN_n sheets (*penta*-B_mN_n),[21, 22] in which only *penta*-BN and *penta*-BN_2 have been confirmed with dynamical stability from the phonon spectra, formation energy analysis, molecular dynamic simulation and mechanical stability analysis. The band structures show that *penta*-BN is an indirect bandgap semiconductor, while *penta*-BN_2 is metallic. In contrast to the six B_mP_n compounds, the structures with dynamical stability are all semiconductors.

7. References

1 H. Yao, L. Ouyang and W.-Y. Ching, *J. Am. Ceram. Soc.*, 2007, **90**, 3194-3204.

2 R. Hill, *Proc. Phys. Soc. Lond.*, 1952, **65**, 349-354.

3 J. Bardeen and W. Shockley, *Phys. Rev.* , 1950, **80**, 72-80.

4 J. Xi, M. Long, L. Tang, D. Wang and Z. Shuai, *Nanoscale*, 2012, **4**, 4348-4369.

5 N. Wang, M. Li, H. Xiao, H. Gong, Z. Liu, X. Zu and L. Qiao, *Phys. Chem. Chem. Phys.*, 2019, **21**, 15097-15105.

6 R. Li, Q. Shao, E. Gao and Z. Liu, *Extreme Mech. Lett.*, 2020, **34**, 100615.

7 M. Born, K. Huang and M. Lax, *Am. J. Phys.*, 1955, **23**, 474-474.

8 K.-A. N. Duerloo, M. T. Ong and E. J. Reed, *J. Phys. Chem. Lett.*, 2012, **3**, 2871-2876.

9 M. Yagmurcukardes, R. T. Senger, F. M. Peeters and H. Sahin, *Phys. Rev. B*, 2016, **94**, 245407.

10 F. Liu, P. Ming and J. Li, *Phys. Rev. B*, 2007, **76**, 064120.

11 R. C. Andrew, R. E. Mapasha, A. M. Ukpong and N. Chetty, *Phys. Rev. B*, 2012, **85**, 125428.

12 M. Topsakal, S. Cahangirov and S. Ciraci, *Appl. Phys. Lett.*, 2010, **96**, 091912.

13 W.-C. Hu, Y. Liu, D.-J. Li, X.-Q. Zeng and C.-S. Xu, *Comput. Mater. Sci.*, 2014, **83**, 27-34.

14 Y. Cai, G. Zhang and Y.-W. Zhang, *J. Am. Chem. Soc.*, 2014, **136**, 6269-6275.

15 K. Kaasbjerg, K. S. Thygesen and K. W. Jacobsen, *Phys. Rev. B*, 2012, **85**, 115317.

16 B. Radisavljevic, A. Radenovic, J. Brivio, V. Giacometti and A. Kis, *Nature Nanotech.*, 2011, **6**, 147-150.

17 J. Xiao, M. Long, X. Zhang, D. Zhang, H. Xu and K. S. Chan, *J. Phys. Chem. Lett.*, 2015, **6**, 4141-4147.

18 A. N. Rudenko, S. Brener and M. I. Katsnelson, *Phys. Rev. Lett.*, 2016, **116**, 246401.

19 B. Huang, H. L. Zhuang, M. Yoon, B. G. Sumpter and S.-H. Wei, *Phys. Rev. B*, 2015, **91**, 121401.

20 Y. Wang, M. Miao, J. Lv, L. Zhu, K. Yin, H. Liu and Y. Ma, *J. Chem. Phys.*, 2012, **137**, 224108.

21 J. Li, X. Fan, Y. Wei and G. Chen, *Sci. Rep.*, 2016, **6**, 31840.

22 L. Z. Liu, Q. T. Pang and Y. Liu, *Mater. Sci. Forum*, 2018, **913**, 573-581.